SEDIMENTOLOGY the journal of the International Association of Sedimentologists

Sedimentology (2022) doi: 10.1111/sed.12976

Preservation of Fe/Mn-redox fronts in sediments of an oligotrophic, oxygenated deep-water lake (Lago Fagnano, Tierra del Fuego)

INA NEUGEBAUER*,† , CAMILLE THOMAS* , LUIS ORDOÑEZ* , NICOLAS D. WALDMANN‡ , CRISTINA RECASENS*, ALEXIS VIZCAINO§ , FRANCISCO J. JIMENEZ-ESPEJO¶,** and DANIEL ARIZTEGUI*

**Department of Earth Sciences, University of Geneva, Rue des Maraichers 13, 1205 Geneva, Switzerland (E-mail: inaneu@gfz-potsdam.de)*

†Section Climate Dynamics and Landscape Evolution, GFZ German Research Centre for Geosciences, Telegrafenberg, 14473 Potsdam, Germany

‡Dr Moses Strauss Department of Marine Geosciences, Charney School of Marine Sciences, University of Haifa, Mount Carmel, 3498838 Haifa, Israel

§Department of Environmental Earth System Science, Stanford University, 67 Panama St, Stanford, CA 94305, USA

¶Instituto Andaluz de Ciencias de la Terra, UGR-CSIC, Avda. de las Palmeras 4, 18100 Armilla (Granada), Spain

***Biogeochemistry Center, Japan Agency for Marine-Earth Science and Technology, Natsushima-cho 2-15, Yokosuka, 237-0061, Japan*

Associate Editor – Lauren Birgenheier

ABSTRACT

Changing redox conditions in water columns or sediment–water interfaces of lakes are captured as sedimentary archives, and are often influenced by climate. Their study therefore permits the reconstruction of past climate change on (sub-) annual to longer timescales. In Lago Fagnano (54°S Argentina/Chile), a large oligotrophic and deep-oxygenated lake, alternations of light grey clay and dark greenish and black laminae are preserved throughout the Holocene sedimentary record. This study aims to clarify the mechanism of laminae formation and preservation in Lago Fagnano, and their relation to changing redox conditions in the lake. High-resolution major element scanning and mapping along with detailed mineralogical analyses of sediment cores allowed identifying Fe-oxides, Mn-oxides and Fe-(mono) sulphides as responsible for the lamination. Based on the interpretation of redox processes at the current sedimentary redox boundary and of buried palaeo-redox fronts underlying mass-transported deposits, the greenish laminae enriched in Fe-oxides are interpreted as palaeo-redox fronts. The preservation of such former interfaces in Lago Fagnano sediments is most likely promoted by rapid increases of sedimentation due to higher runoff related to stronger Southern Hemisphere Westerlies. The formation of black laminae, showing only traces of Fe-(mono) sulphides and organic matter, is obscured by oxidation and early diagenetic processes, i.e. degradation and partial pyritization. These layers were presumably generated by small changes in bottom-water oxygenation due to reduced mixing and/or higher productivity. This study highlights the value of high-resolution sediment–geochemical analyses to better understand redox and diagenetic processes in oligotrophic mixed lakes.

Keywords Early diagenesis, Fe-/Mn-oxides, mixed lakes, redox fronts, sedimentary geochemistry, southernmost Patagonia, Southern Hemisphere Westerlies.

INTRODUCTION

The sensitivity of lakes to varying environmental conditions, stored in the lacustrine sedimentary record, is widely used in palaeoenvironmental studies (e.g. Bradley, 1999). However, the underlying processes controlling the physicochemical behaviour of lakes, such as mixing, stratification, or the dynamics of redox boundaries in space and time remain complex to understand. For instance, the modern redox boundary between oxidizing and reducing conditions might migrate across the sediment–water interface and thus have a major effect on biogeochemical cycling, such as the type and occurrence of benthic organisms, organic matter preservation and geochemical diagenesis (Davison, 1993; Sobek *et al.*, 2009; Lau *et al.*, 2018). Seasonal cycles of precipitation, thermal gradients and wind intensity are climate factors that can trigger stratification, oxygenation or mixing and might have an impact on the redox status of a lake (Brown *et al.*, 2000). Moreover, an increase in nutrients input may also indirectly cause biological depletion of oxygen and subsequently change the redox status of water bodies (Davison, 1993). The seasonal pattern of these events may also influence the limnology on a longer timescale. Disentangling the forcing mechanisms responsible for these redox changes is necessary to understand the sedimentation and preservation processes in lacustrine sedimentary archives.

Prevalent redox-sensitive elements in sediments (like Fe, Mn, S and As) are preferentially used for understanding redox changes in lakes through time (Davison, 1993; Bryant *et al.*, 1997). In a well-ventilated lake, the water column remains oxygenated at depth, and anaerobic conditions only prevail at the sediment–water interface or few centimetres below. In reducing environments associated with low oxygen, the solubility of Fe and Mn increases, with Mn being far more soluble and migrating away (Burdige, 1993; Davison, 1993; Boyle, 2001). Hence, an increase in sedimentary Fe/Mn ratios can point to the onset of anaerobic conditions due to stratification, or to de-oxygenation from organic decay following enhanced biological activity (Davies *et al.*, 2015). The Mn/Fe ratio, on the other hand, is often used to trace bottom-water oxygenation (e.g. Francus *et al.*, 2013; Naeher *et al.*, 2013).

Various factors can influence the redox conditions in a lake, including changes in water depth, biological productivity, trophic state, alkalinity and sedimentation rate. These changes can occur in response to variability in climate parameters such as temperature, precipitation, wind strength and anthropogenic impact. For instance, low Fe/Mn values in Holocene sediments from Lake Potrok Aike (Argentinian Patagonia) may have resulted from increased lake mixing, either due to lake-level lowering or enhanced wind speed (Haberzettl *et al.*, 2007). At Lake Montcortes in north-east Spain, Fe/Mn ratios were proposed to reflect variations of agricultural runoff that modulate the biological productivity in the lake (Corella *et al.*, 2012). In Lake Baikal, Russia, sedimentary layers are enriched both in Mn and Fe, often forming crusts, and have been interpreted as formed during periods of reduced accumulation of suspended sediments at the transition between glacial and interglacial stages (Granina *et al.*, 1993; Deike *et al.*, 1997; Brown *et al.*, 2000). The underlying factors controlling the Fe/Mn content in a lake are often ambiguous, requiring comprehensive multi-proxy approaches for unequivocal interpretation.

Lago Fagnano is the southernmost large ice-free lake outside Antarctica and, as such, a gateway for understanding past and present relations between Antarctic, South Pacific and South Atlantic climate changes. Analyses of sediments deposited in this lake during the Holocene include sedimentology, geochemistry and micropalaeontology to reconstruct palaeoclimatic and environmental changes, glacier fluctuations and tectonic activity (Waldmann *et al.*, 2008, 2010a, 2010b, 2011, 2014; Moy *et al.*, 2011). These studies demonstrate that the sediments deposited in Lago Fagnano are a sensitive and reliable recorder of past climate variability in the southern high latitudes. Strong Southern Hemisphere westerly winds impact Lago Fagnano, especially during austral summer, favouring deep ventilation (Waldmann *et al.*, 2014). Still, the sediments exhibit a cyclic alternation of light grey clay

and Fe-rich greenish and black laminae throughout the Holocene. It has been suggested that Fe-rich laminae result from temporary oxygen depletion at the lake bottom when the Southern Hemisphere westerlies are weaker in the region of Tierra del Fuego (Waldmann *et al.*, 2010a). Nevertheless, the causes and frequency of the formation of these Fe laminae in Lago Fagnano are unknown, limiting further interpretation regarding changing redox conditions and palaeoclimatic response of the lake.

Similar Fe-rich laminae have been described from other oligotrophic and well-ventilated deep lacustrine environments comparable to Lago Fagnano, for instance Lake Ohrid in Albania/Macedonia (Vogel *et al.*, 2010), Loch Lomond in Scotland (e.g. Farmer, 1994), Lake Malawi (Brown *et al.*, 2000), and particularly Lake Baikal, where active and preserved Fe/Mn-layers form peculiar crusts and have been extensively studied (e.g. Granina *et al.*, 1993, 2004, 2010, 2011; Deike *et al.*, 1997; Müller *et al.*, 2002; Och *et al.*, 2012; Torres *et al.*, 2014). Granina *et al.* (2004) suggested that Fe/Mn-layers in Lake Baikal sediments can be used as a proxy for periods of low sedimentation rates and well-oxygenated conditions, and that these ancient redox fronts were buried by rapid changes in sedimentation regime. The same mechanism was proposed for concretionary Fe/Mn-horizons observed in sediments of Lake Ohrid (Vogel *et al.*, 2010) and Lake Malawi (Brown *et al.*, 2000). At Lake Baikal and Lake Ohrid, lake conditions under which these redox fronts form and are preserved are comparable to Lago Fagnano, i.e. a deep-water, oligotrophic, well-mixed setting with generally low productivity and sedimentation rates.

In this study, high-resolution sedimentological and geochemical data of drilled sediment cores from Lago Fagnano are presented to explain the mechanism of the Fe-rich laminae formation and preservation in the lake. Their composition and occurrence are analysed to identify the factors controlling their formation and mechanisms behind changing patterns in redox conditions in Lago Fagnano during the Holocene. New perceptions about early diagenetic processes and changing redox conditions developed from this study are applicable to similar oligotrophic and deep-ventilated lacustrine settings and can help to resolve reconstructions based on diagenetically influenced palaeoclimatic proxies.

STUDY AREA

Lago Fagnano [54°S, *ca* 68°W; 26 m above sea level (asl)] is located on the Tierra del Fuego archipelago in southernmost Patagonia (Fig. 1). The *ca* 105 km east–west elongated and 10 km wide lake basin has evolved as a continental pull-apart structure that was deepened by subsequent Pleistocene glacial activity (Waldmann *et al.*, 2008). The geology to the south and north of the lake is mainly composed of black shale and whitish-grey tuff successions of the Sierras de Alvear, and marine greywacke of the Sierras de Beauvoir, respectively (Olivero & Martinioni, 2001; Tassone *et al.*, 2005). Large amounts of terrigenous elements, like Fe and Ti, are delivered to Lago Fagnano by weathering of these rocks and fluvial and aeolian influx (Gaiero *et al.*, 2003).

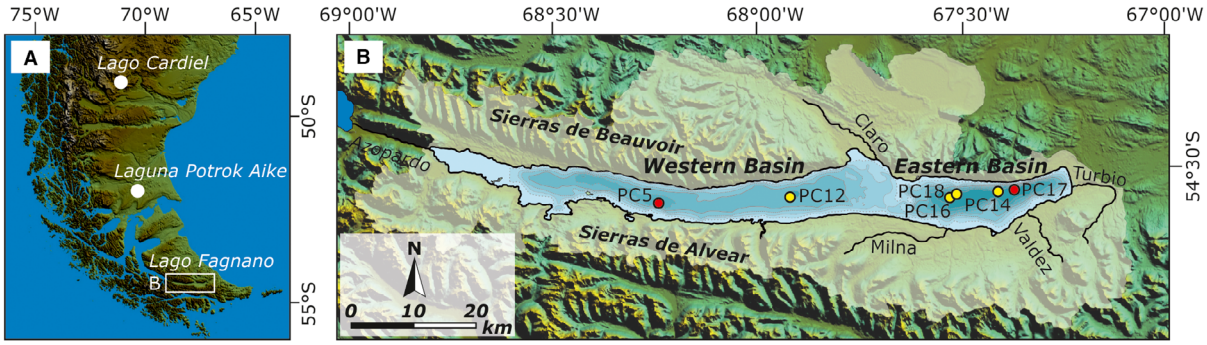

Fig. 1. Regional setting of Lago Fagnano. (A) Location of Lago Fagnano (white box) on Tierra del Fuego and other lake records in southern South America; (B) Bathymetric map (water depth contours in equidistant 25 m steps; solid line—100 m) and watershed (white-shaded area) of Lago Fagnano including coring locations of cores analysed here (LF06-PC5 and LF06-PC17; red dots) and from previous studies (Waldmann *et al.*, 2010a; Moy *et al.*, 2011; yellow dots).

Lago Fagnano is divided into a smaller eastern sub-basin with a maximum water depth of 210 m and a larger, shallower western-central sub-basin of maximum 130 m water depth (Fig. 1). The principal rivers flowing into the lake from the south and east are Río Milna, Río Valdez and Río Turbio, whereas only Río Claro drains into the central lake basin, coming from the north. One fluvial outlet, Río Azopardo, drains the lake at its westernmost extreme into the Almirantazgo Fjord (Admiralty Sound) towards the Strait of Magellan.

Owing to the harsh weather conditions in the region, information about the recent limnology of the lake is limited. The high degree of water transparency, low algal biomass and nutrient content indicate an ultra-oligotrophic to oligotrophic status (Quirós & Drago, 1999). Water column measurements every 5 to 20 m from two locations in the western sub-basin and one from the eastern sub-basin carried out in November 2006 revealed only small changes in pH (*ca* 7.8), temperature (*ca* 6°C) and oxygen content (*ca* 6 to 12 mg l^{-1}) and no significant thermocline, which suggests well-mixed conditions during this austral spring season (Waldmann *et al.*, 2014). Mixing and oxygenation of the water column was likely induced by heavy precipitation prevailing at that time and leading to a *ca* 1.5 m higher than normal lake level (Waldmann *et al.*, 2014). It has been suggested that the higher lake level may have caused flooding and erosion of coastal areas, leading to an increased concentration of detrital material in the water column across the lake and potentially favouring vertical mixing (Waldmann *et al.*, 2014).

The climate in Tierra del Fuego is sub-polar, with moisture originating from the Pacific Ocean, modulated by the south-east Pacific subtropical anticyclone and the circum-Antarctic low-pressure belt (Rogers & Loon, 1982). During austral summers, intense precipitation and increased zonal winds are forced by the southward migration of the Southern Hemisphere Westerlies (SHW) to the region (Lamy *et al.*, 2001; Garreaud *et al.*, 2013). The cold and relatively drier austral winters are mostly influenced by the Antarctic Oscillation (AO) system (Gong & Wang, 1999).

MATERIAL AND METHODS

Sediment cores

The drilling campaign at Lago Fagnano was carried out in 2006 (Waldmann *et al.*, 2010a) and retrieved a series of 18 piston cores up to 8 m length using a Kullenberg-type coring system. All cores were scanned at ETH Zürich, Switzerland, with a GEOTEK^{TM} multi-sensor core logger (MSCL; Geotek Limited, Daventry, UK) to obtain their petrophysical properties (magnetic susceptibility, wet bulk density and P-wave velocity). The present study included sediment cores LF06-PC5 (126 m water depth) and LF06-PC17 (195 m water depth) from the western and eastern sub-basins of Lago Fagnano, respectively (Fig. 1B). These cores were retrieved in the vicinity of previously studied seismic profiles and core sequences (Waldmann *et al.*, 2010a; Moy *et al.*, 2011), which allows for a good correlation with these cores. Core LF06-PC5 is 2.12 m long and presents grey and black sediment laminae in the upper 1.42 m, which represents the studied sequence in this contribution. The Hudson H1 tephra (7683 ± 33 ^{14}C yr BP; Stern *et al.*, 2016), identified in several cores of Lago Fagnano (Waldmann *et al.*, 2010a) including core LF06-PC5 as a *ca* 3 cm thick deposit at 1.16 m depth, is used as tephrochronological anchor. Core LF06-PC17 is 8.51 m long, with the lower 6.47 m containing slumped deposits and the uppermost 2.04 m consisting of undisturbed and finely laminated sediments, and thus suitable to be used in this study. Core LF06-PC17 preserves several event marker-layers that allowed correlation to previously established event stratigraphy based on the nearby core LF06-PC16 (Table 1; Figs 1B and S1; Waldmann *et al.*, 2011, 2014).

Radiocarbon dating

Previous attempts to establish age models for sediment cores from Lago Fagnano (LF06-PC12, LF06-PC16 and LF06-PC18; Fig. 1B) were based on the H1 tephra age (Stern, 2008; refined in Stern *et al.*, 2016) and Accelerator Mass Spectrometry (AMS) radiocarbon dating of bulk organic sediments, terrestrial macrofossils and pollen concentrates (Moy *et al.*, 2011; Waldmann *et al.*, 2011). The latter were found to produce the most reliable results for sediments from Lago Fagnano, whereas ages obtained from bulk sediments were 5000 to 7000 years older, most likely due to contamination with radiocarbon-dead material. The scarce terrestrial macrofossils that are mostly associated with mass-flow events are presumably redeposited from the basin slopes and produced old ages as well (Moy *et al.*, 2011).

To obtain independent age models for the sediment cores investigated here, a total of six samples

Table 1. Event stratigraphy of mass-transported deposits in the eastern sub-basin of Lago Fagnano. Events of core LF06-PC17 (this study) were correlated to the published stratigraphy in cores PC16 and PC14 (Events C15–C24; Waldmann *et al.*, 2011) and to core PC18 (Moy *et al.*, 2011); see Fig. S1 for illustration.

Event stratigraphy		PC16	PC18	PC14	PC17		
Event	Linear age (yr BP)	Sediment depth (cm)	Sediment depth (cm)	Sediment depth (cm)	Event	Linear age (yr BP)	Sediment depth (cm)
C24	56	1.8–6.1	1.8–14.9	0.0–0.2	#17-1	−12	2.3–6.0
C23	574	35.6–37.7	35.4–37.8	11.2–14.9	#17-2	570	36.5–39.2
C21	1111	72.3–85.3	54.8–66.6	39.7–46.3	#17-3	1090	66.3–75.3
C19	1814	117.2–119.3	77.4–79.3	71.8–79.3	#17-4	1780	111.5–122.0
C18	2702	172.6–174.3	99.9–101.7	136.6–147.2	#17-5	2240	135.5–147.9
C17	–	177.6–184.8	–	150.3–159.2	–	–	–
C16	3311	–	–	195.2–207.4	#17-6	3310	203.9–216.4
C15	4053	251.3–258.8	130.0–131.8	259.8–273.5	–	–	–

of pollen concentrates were prepared from the bottom, middle and top parts of the laminated intervals from cores LF06-PC5 and LF06-PC17 (Table 2). Considering the low total organic carbon content (<1.2%) of Lago Fagnano sediments (Waldmann *et al.*, 2010a; Fig. S1), and to assure that the minimum amount of carbon and pollen required for AMS dating could be extracted, relatively thick (3 to 9 cm) slices of sediment were sampled. The extraction followed several physical and chemical separation steps mainly after Brown *et al.* (1989), Nakagawa *et al.* (1998) and Regnéll & Everitt (1996). The protocol included sieving with 250 μm and 6 μm meshes, treatment with heated HCl, KOH and H_2SO_4, and heavy-liquid density separation using CsCl and SPT (sodium polytungstate). After microscopic inspection of the remaining respective individual fractions, those containing mainly terrestrial organic micro-remains were merged and separation steps were repeated until no further purification was possible. AMS dating of the residual samples of organic micro-remains was done at the Poznan Radiocarbon Laboratory, Poland.

X-ray fluorescence element scanning and mapping

Continuous semi-quantitative elemental composition of the sediment cores was determined by non-destructive micro-X-ray fluorescence (μ-XRF) scanning on the split-core sediment surface using an ITRAX elemental scanner (COX Analytical Systems, Mölndal, Sweden; Croudace *et al.*, 2006) at the University of Bern, Switzerland. Both, a Cr-tube to capture variations of relatively lighter elements (Al, Si, S, K, Ca and Ti) and a Mo-tube for the proper detection of Mn and heavier elements (Fe, As, Rb, Sr and Zr) were used, operated at 30 kV, 50 mA and 50 s exposure time per step. Typically, an exposure time of 7 to 10 s would be sufficient to get reliable results for silt-rich and clay-rich lake sediments (Löwemark *et al.*, 2018). Here, a five-fold higher exposure time was chosen to ensure robust sulphur counts, which have been recorded with only low counts per second in Lago Fagnano sediments previously (Waldmann, 2008). To reduce any migration of mobile elements, the sediment cores were measured within a few weeks after core opening and the oxidized surface layer of the sediment cores (typically less than 1 mm thick) has been removed before each scan. The relatively coarser lamination of core LF06-PC5 and the finely laminated sediments of core LF06-PC17 were scanned in contiguous 1.0 mm and 0.5 mm increments, respectively. Element intensities are presented as centred log-ratios [clr = ln (element intensity/geometric mean of range of elements)] or log-element ratios to account for sediment-matrix and water-content effects (Tjallingii *et al.*, 2007; Weltje & Tjallingii, 2008).

For high-resolution characterization of the elemental distribution within the laminated sediments, elemental mapping of exemplary *ca* 1.5 cm × 1.0 cm sized areas was performed on impregnated and polished sediment blocks

Table 2. Radiocarbon dates of organic micro-remains extracted from cores LF06-PC5 and LF06-PC17

Lab-ID POZ-	Sample-ID (core_section_cm)	Core depth (m)	Event-free core depth (m)	Material	Age (^{14}C yr BP ± error)	Calibrated age (cal yr BP ± 1σ)
95359	PC5_2/2_10-14	0.12	0.12	40–50% charred particles 30–40% cf. phytoliths 10–20% pollen and spores 5–10% Pediastrum	8220 ± 50	9186 ± 87
95361	PC5_2/2_55-59.5	0.57	0.555	30–40% charred particles 30–40% algae/Pediastrum 20–30% pollen and spores 5–10% tissues 5–10% minerogen. particles	6520 ± 70	7434 ± 70
NN	PC5_1/2_21-24	1.16	0.91	Hudson (H1) tephra*	7683 ± 33	8469 ± 39
95360	PC5_1/2_41-50	1.38	1.125	50–60% pollen and spores 20–30% charred particles 10–20% minerogen. particles 10% algae	10 870 ± 60	12 751 ± 50
95357	PC17_6/6_8-14	0.11	0.07	60–70% tissues 30–40% charred particles 10% pollen and spores Few fungal remains	6720 ± 40	7588 ± 37
95358	PC17_6/6_95-99	0.97	0.815	50–60% tissues 30–40% charred particles 10% pollen and spores 10% fungal remains Few minerogen. particles	6100 ± 40	6973 ± 79
95355	PC17_5/6_47-52	1.96	1.68	40–50% tissues 30–40% pollen and spores 20% charred particles 5% algae	12 680 ± 70	15 090 ± 140

* Stern *et al.* (2016), mean age obtained from bulk sediment AMS ^{14}C dating from different lakes.

using an EAGLE III μ-XRF spectrometer (EDAX Inc., Mahwah, NJ, USA) at the University of Geneva, Switzerland. The device was employed with a Rh-tube operated with 40 kV voltage, 375 to 675 μA current, very short dwell times of 4 to 10 ms per spot, and overlapping 50 μm spot sizes in *ca* 24 μm steps. Elemental overlay images were produced using the EAGLE-internal evaluation software.

Scanning electron microscopy and X-ray diffraction analyses

Ten samples were taken from characteristic sediment laminae and dried for mineralogical analyses. Aliquots were ground and prepared for powder X-ray diffraction (XRD) analyses using a PANalytical-Empyrean X-ray diffractometer (Malvern Panalytical, Malvern, UK) at the University of Geneva, Switzerland. A continuous scan mode was applied using Bragg-Brentano geometry, a step size of 0.013°2θ and a counting time/step of 350 s in the range of 4 to 70°2θ with a Cu anode at 45 kV and 40 mA. Peaks were identified using the PANalytical HighScore Plus software.

For identification of different Fe and Mn phases in the sediments, ten aliquots were also inspected with a Jeol® JSM-7001 FA scanning electron microscope (SEM; JEOL, Tokyo, Japan) at the University of Geneva, Switzerland, equipped with an energy dispersive X-ray analyser (EDS JED2300). After a first analysis, clay minerals were partially removed by centrifugation, allowing for improved observation of heavier fractions.

Thin section and image analysis

For microscopic inspection of different characteristics of laminated sediments along the analysed

sediment cores, 20 petrographic thin sections of 10 cm length each were prepared at MKfactory (Germany). Standard protocols for thin section preparation of soft sediments were applied (e.g. Brauer *et al.*, 1999), including freeze-drying and impregnation with epoxy resin (Araldite 2020). Thin sections were investigated using a petrographic microscope with varying magnifications (25× to 400×) and optical conditions (plane parallel/semi-polarized/polarized light).

RESULTS

Sediment cores and age-depth models

Western-central basin core LF06-PC5

The 2.12 m long core LF06-PC5 is divided into two lithological units (LU1 and LU2; Fig. 2A). LU2 (2.12 to 1.42 m depth) is characterized by homogeneous, light grey clayey to silty mud, a relatively high density of *ca* 1.8 g cm^{-3} and magnetic susceptibility values of *ca* 20 × 10^{-5} SI. LU1 (1.42 to 0 m depth) preserves millimetre to centimetre-scale greenish and black laminae within an overall light grey mud, and decreasing density and magnetic susceptibility towards the top of the unit. Five graded event beds of 1.5 to 19 cm thickness (labelled #5-1 to #5-5) and a 3 cm thick tephra layer (H1) at 1.16 m depth are clearly identified by distinct high density and magnetic susceptibility values (Fig. 2A).

Radiocarbon dating of organic micro-remains returned ages of 10 870 ± 60, 6520 ± 70, and 8220 ± 50 ^{14}C yr BP for the bottom, middle and top of LU1, respectively (Table 2). Because these ages are considerably older than the well-dated H1 tephra age (7683 ± 33 ^{14}C yr BP (Stern *et al.*,

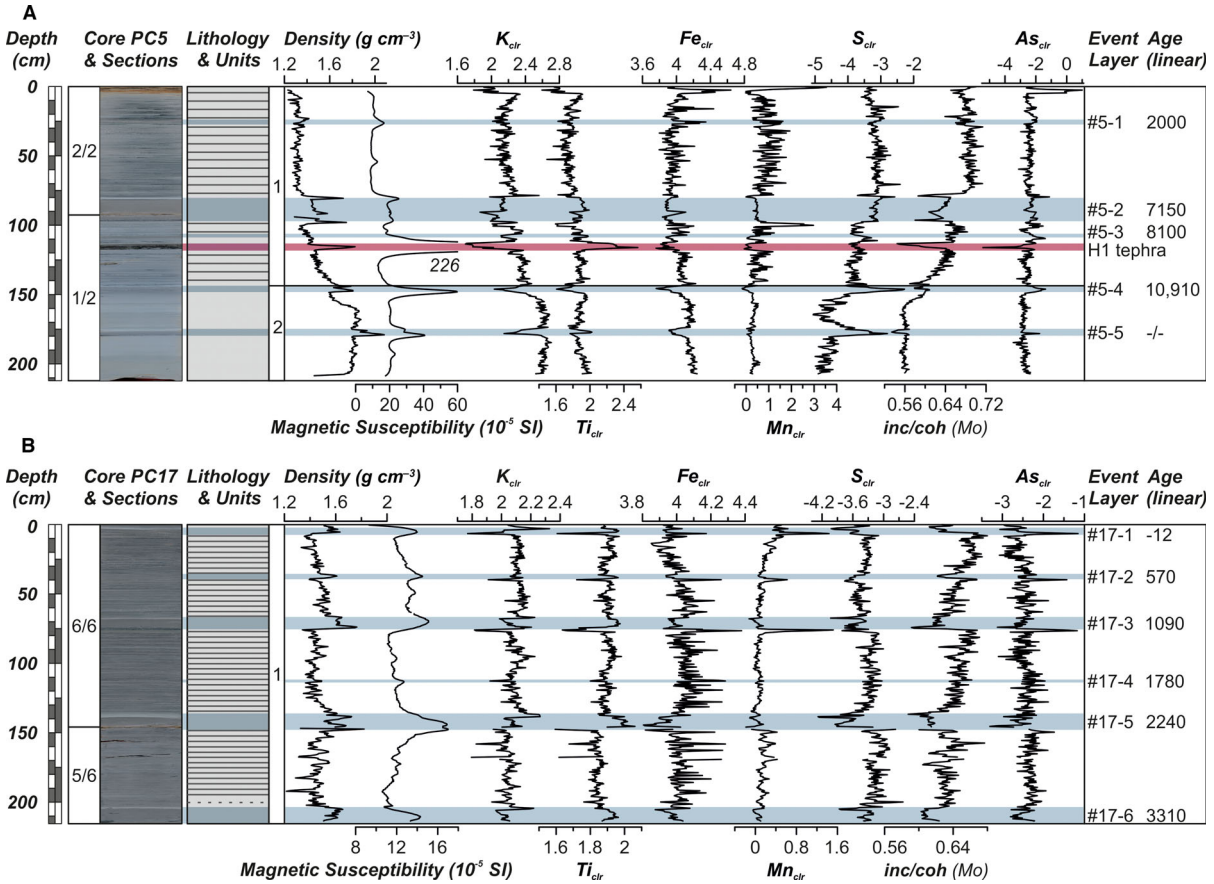

Fig. 2. Lithology, density, magnetic susceptibility, μXRF, event layers and age estimates of cores (A) LF06-PC5, and (B) LF06-PC17 in the western and eastern sub-basins, respectively. X-ray fluorescence (XRF) data are given as centred log-ratios (clr). Ages for event layers (blue bars) were calculated by linear interpolation based on the H1 Hudson tephra age (Stern *et al.*, 2016) for core LF06-PC5, and event stratigraphy for core LF06-PC17 following Waldmann *et al.* (2011; applying a constant sedimentation rate of 0.52 mm/yr; see text for further explanation).

2016), calibrated to 8469 ± 39 yr BP), the age model of core LF06-PC5 is based on linear interpolation and extrapolation using only the tephra. Following this approach, the laminated LU1 of core LF06-PC5 was deposited during the last *ca* 10 900 years (Fig. 2A) with a sedimentation rate of 0.11 mm yr^{-1} (event-layers excluded).

Eastern basin core LF06-PC17

The upper 2.04 m of core LF06-PC17 (Fig. 2B) preserves undisturbed alternations of millimetre-scale greenish or black and light grey, clayey-silty laminae with relatively constant density (1.3 to 1.5 g cm^{-3}) and magnetic susceptibility (10 to 12 × 10^{-5} SI) values that are comparable to those measured in LU1 of LF06-PC5 (Fig. 2A). Six graded event beds of 0.5 to 12.5 cm thickness (labelled #17-1 to #17-6) have been identified in LU1 by elevated density and magnetic susceptibility values. These clastic layers are typically characterized by a dark grey, coarse silty to sandy base followed by upward fining and a whitish clay top, and have been interpreted as mass-transport deposits triggered by earthquakes (Waldmann *et al.*, 2011).

Similar to the western basin, radiocarbon dating of organic micro-remains from the bottom, middle and top parts of the undisturbed laminated top-section of core LF06-PC17 resulted in too old ages (Table 1). The accurate transfer of published ^{14}C ages obtained from core LF06-PC18 (Fig. 1; Moy *et al.*, 2011) to this core was accompanied by caveats in the proper correlation (Fig. S1). Therefore, the age model for core LF06-PC17 is based on correlating the event stratigraphy with the published record from the nearby core LF06-PC16 (Waldmann *et al.*, 2011) (Table 1; Fig. S1). Furthermore, this correlation approach was extended to core LF06-PC14, as there is no accurate age for the bottommost event in core LF06-PC16 (C16; Waldmann *et al.*, 2011). Linear interpolation between events C18 and C15 resulted in an age estimate of 3310 yr BP for event C16, which is equivalent to event #17-6 in core LF06-PC17 (Table 1; Fig. S1). Hence, the bottom of the laminated section of core LF06-PC17 can be estimated with such an age. A constant sedimentation rate of *ca* 0.52 mm yr^{-1} is calculated for core LF06-PC17, when event layers are extracted and considered as non-erosive, which is confirmed in thin sections (Fig. 6B).

Sediment composition and elemental characteristics

Sediments of both investigated cores are predominantly clastic and composed of clay and silt, as well as fragmented and mostly centric diatoms (of the genus *Discostella*; Waldmann *et al.*, 2014). XRD and SEM analyses reveal a monotonous and similar composition for both cores, regardless of the presence of laminae. The composition is characterized by illite-type clay minerals, quartz, albite (plagioclase feldspar) and chlorite (phyllosilicates). Birnessite (Mn-oxide) and Fe-oxide were detected in the top 5 cm of core LF06-PC5 by both XRD and SEM. These oxides appear as amorphous, *ca* 5 to 15 μm sized conglomerated sheets (Fig. 3).

The dominance of clastic sediments is also reflected in the XRF elemental composition of the laminated parts of the core profiles (respective LU1 in cores LF06-PC5 and LF06-PC17; Fig. 2). Iron is by far the dominant element, with four-

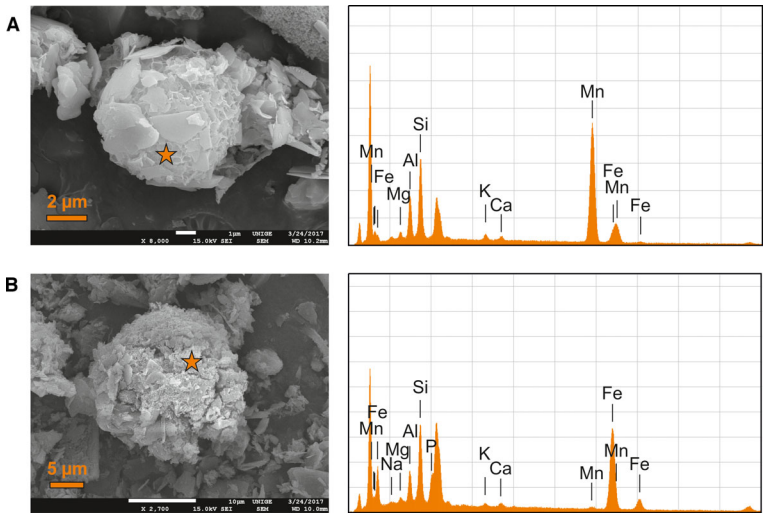

Fig. 3. Scanning electron microscopy (SEM) photographs of (A) Mn-oxide (core LF06-PC5 at 1 cm sediment depth) and (B) Fe-oxide (core LF06-PC5 at 3 cm sediment depth) with corresponding energy dispersive X-ray analyser (EDS) spectra. Orange stars denote the measurement positions. Note that clay minerals partly cover the oxides, producing minor peaks of, for example, Si, Al and K in the EDS spectra.

fold higher counts (on average 30 000 counts per second, cps) than the geometric mean of the considered elements. Lowest counts were recorded for S and As (Fig. 2) with on average *ca* 20 cps for S and *ca* 60 cps for As. Core LF06-PC5 shows an overall decrease of density and detrital elements (K and Ti), and an increase of S and inc/coh over the non-laminated bottom-part towards the top, stabilizing above *ca* 80 cm sediment depth. For the elements Fe, Mn and As in LF06-PC5, and for all parameters of LF06-PC17, hardly any trends are observed. Instead, varying intensities of the elements for which centred log-ratios were calculated (Al, Si, S, K, Ca, Ti, Mn, Fe, As, Rb, Sr and Zr) are mainly associated with the occurrence of mass-transported deposits and the pattern of light grey and dark greenish or black laminations (see Figs 5 and 6, and their description below). In particular, underlying the well-graded mass-transported events in LF06-PC17, distinct negative peaks of K and Ti are observed, whereas Fe, Mn, As and the incoherent (Compton)/coherent (Rayleigh) scattering ratio of the XRF device (inc/coh ratio) show strong positive excursions.

After extraction of the event layers from the XRF profiles in cores LF06-PC5 and LF06-PC17, principal component analysis (PCA) was applied to the normalized data, as well as to the element-ratios Fe/K, Mn/K, Mn/Fe and inc/coh retrieved from the Mo-tube and Cr-tube, respectively (Fig. 4). For both cores, the first two principal components (PC1 and PC2) explain about 60% of the observed variance in the XRF data. Considering also correlation coefficients (Table S1), the regarded elements and ratios describe two main inter-relations:

1 The first principal component (PC1) shows a counter-relation between elements that are bound to minerogenic clay and associated detrital minerals [Al, Si, K, Ca, Ti, (Rb, Sr and Zr only in core PC5); red in Fig. 4] and parameters that are associated with sediment components formed in the lake. To discriminate between potential authigenic/diagenetic and detrital Fe and Mn phases, these two elements were normalized against K, which shows the highest counting and correlation values amongst the allogenic elements. Fe/K and Mn/K correlate well ($r \geq 0.89$) with Fe and Mn, respectively, implying the dominance of authigenic or diagenetic phases in the sedimentary record. In the western-basin core LF06-PC5, a slightly weaker correlation between Fe/K and Fe ($r = 0.71$), as well as an insensitivity of Fe to reflect the first principal component (Fig. 4) are observed, indicating the presence of some detrital Fe-phases. In LF06-PC17, minerogenic detritus elements build two clusters, with Rb, Sr and Zr potentially reflecting a fraction of the hemipelagic sediments with mixed grain sizes (Davies *et al.*, 2015). This discrimination is less obvious in core LF06-PC5. The positive correlation of S and As with Fe/K in both sediment cores points towards their common binding within Fe-sulphide. Furthermore, in both cores Fe/K, S and As correlate well with the incoherent/coherent scattering ratio, which resembles the average atomic number of the sediment matrix composition. Since organic carbon has a lower atomic number than the measurable elements, this ratio can be used as a qualitative estimation of the

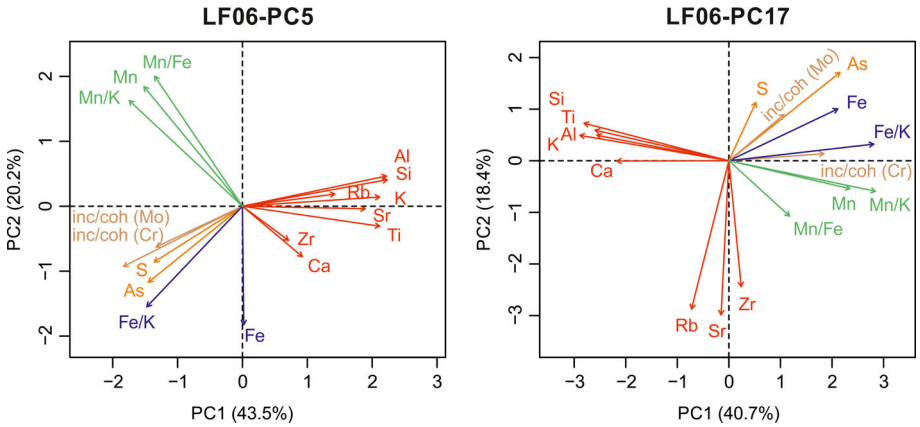

Fig. 4. Principal component-biplots of X-ray fluorescence data for the laminated sections of cores LF06-PC5 and LF06-PC17. Mass-transported deposits were excluded from the datasets.

organic content of the sediment (e.g. Burnett *et al.*, 2011).

2 The second principal component (PC2) describes the relation between non-detrital Fe (associated with S, As and inc/coh) and Mn (Fig. 4) that are susceptible to changing reducing or oxidizing (redox) conditions. This relation is stronger in core LF06-PC5 than in core LF06-PC17. The cluster of Fe/K, S, As and inc/coh can be explained by element affinity for Fe-sulphides

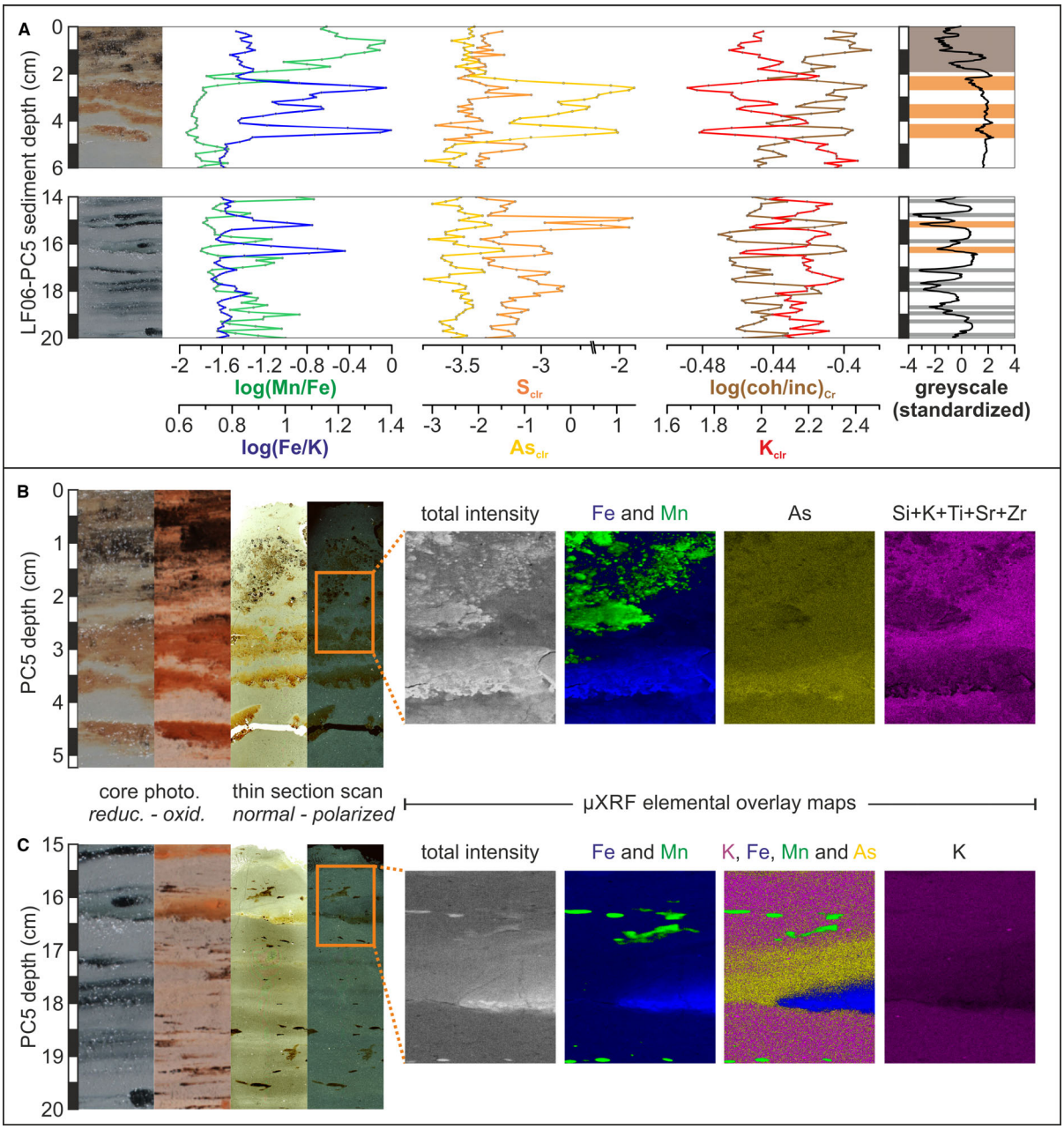

Fig. 5. Characterization of the lamination pattern in the western-central sub-basin of Lago Fagnano (core LF06-PC5). (A) X-ray fluorescence (XRF) element scans of Mn/Fe, Fe/K, S, As, coh/inc and K for 0 to 6 cm and 14 to 20 cm sediment depth (expressed as log-ratio or clr = centred log-ratio), and standardized greyscale of the core image that allowed defining laminae (brown: topmost Mn-enrichment, orange bars: orange (top) or greenish Fe-oxide laminae, grey bars: black laminae); (B) and (C): core photographs, thin section scans and µXRF elemental overlay maps of (B) the top-core brownish-black Mn-oxides and orange-brown Fe-oxides, and (C) an exemplary greenish Fe-oxide lamina, followed by As enrichment and Mn patches.

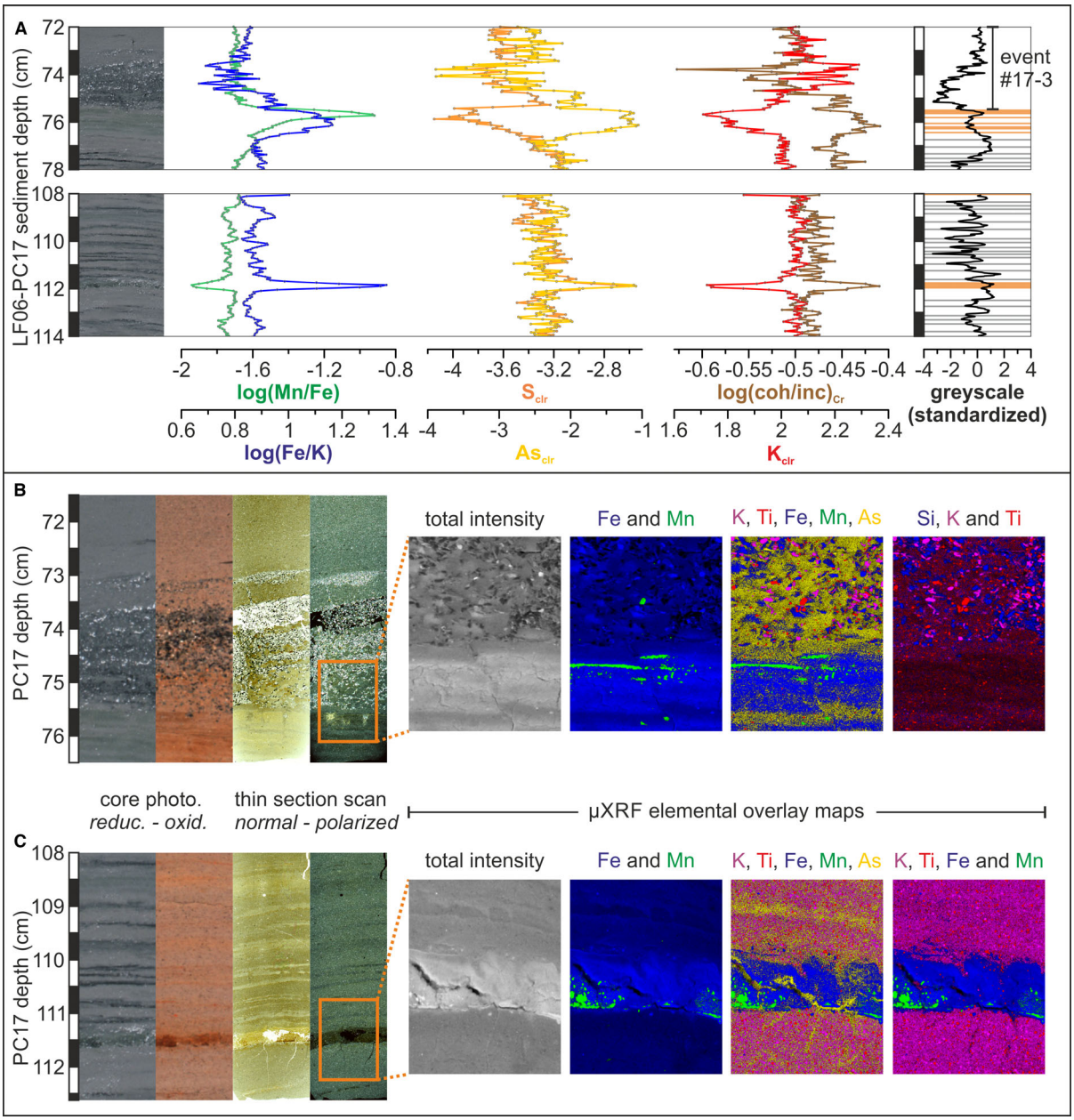

Fig. 6. Characterization of the lamination pattern in the eastern sub-basin of Lago Fagnano (core LF06-PC17). (A) As in Fig. 5, but for different depth intervals (72 to 78 cm and 108 to 114 cm); (B) and (C): core photographs, thin section scans and µXRF elemental overlay maps of (B) greenish, Fe and Mn-enriched laminae followed by the coarse-grained base of a graded layer (event #17-3), and (C) an exemplary greenish Fe-oxide lamina (at 111.5 cm depth) that is enriched in As, S [not detectable by XRF mapping, but distinct S-peak in (A)] and some Mn, and a thin As-elevated black lamina (at 111 cm depth).

and organic matter, hence implying reducing conditions. The Mn/Fe ratio, which indicates oxidation, shows no correlation or a very slight anti-correlation with Fe/K (Table S1), which becomes stronger only when Fe/K shows peaks on the lamina-scale (Figs 5 and 6).

Characterization of the sediment lamination

The light grey and greenish or black lamination patterns observed in the sediment cores of Lago Fagnano were inspected by thin section microscopy, and µXRF elemental scanning and

mapping. The laminated packages found in the two sub-basins show overall similar sedimentary and elemental characteristics (Figs 5 and 6).

Lamination in the western-central sub-basin (LF06-PC5)

Core LF06-PC5 presents a continuous, few millimetres to centimetre-scaled lamination pattern of black and greenish clay layers (on average every *ca* 5 mm) embedded within the light grey clayey-silty background sediments (Fig. 5). The light grey sediment is dominantly composed of clastic minerals, which is reflected by elevated XRF values of detrital elements (represented by K; Fig. 5A). It is also enriched in Mn in the uppermost *ca* 2 cm of the core (Fig. 5A), where birnessite, a layered manganese oxide detected by XRD and SEM (Fig. 3), is observed as dark brown to black patches (Fig. 5B). Further downcore, such patchy Mn-oxide accumulations are visible within the light grey sediment matrix on the core photograph, in thin sections and in XRF maps, all of which produced a few months after core opening. However, these accumulations are not observed on the fresh split-core surface (Fig. 5C).

Black laminae are often discontinuous and their colour rapidly fades after core opening, i.e. after exposing the sediment to oxygen (Fig. 5C). In the thin sections, black laminae appear faint and particularly fine-grained, hardly contrasting with the clayey sediment (Fig. 5C). Greenish laminae turn orange-brown in colour after oxygen-exposure and can be well-discriminated in thin sections (Fig. 5C). These greenish (black) laminae show distinct (small) positive peaks in Fe, As, S and coh/inc, and negative excursions of Mn and detrital elements (like K; Fig. 5A). The most pronounced Fe-peaks are, however, observed within three orange-brown layers at *ca* 2.5 to 5.0 cm depth (Fig. 5B) that underlie the Mn-enriched brownish patches at the top of the core.

Lamination in the eastern sub-basin (LF06-PC17)

Fine millimetre-scaled laminations are observed in core LF06-PC17 (eastern sub-basin; Fig. 6). Like in the western-central sub-basin, the laminated section of the core consists of fine-grained and faint black and greenish laminae, yet their frequency is higher (*ca* 2 mm). As in LF06-PC5, black laminae become less distinct once oxidized after core opening, whereas greenish laminae become more apparent (Fig. 6C). The elemental distribution within the laminae in core LF06-PC17 is comparable to that of the western basin as well, with detrital elements (for example, K; Fig. 6A) and Mn/Fe being enriched in the light grey clayey-silty sediment, and peaks of Fe, As, S and coh/inc in the thin black and greenish laminae. A different behaviour is observed for greenish laminae preceding mass-transport deposits, where Fe and Mn are enriched and S is depleted (Fig. 6A and B). The enrichment of Mn, Fe and As within brownish black Mn-oxide and brownish orange Fe-oxide layers at the top of the western-basin core (LF06-PC5; Figs 2 and 5) is not observed in core LF06-PC17. However, in the nearby eastern-basin core LF06-PC16, a thin orange-brown layer is observed at *ca* 2.5 cm depth, at the top of the mass-transport event C24 (i.e. event #17-1 in core LF06-PC17; Fig. S1).

DISCUSSION

Age model construction

Radiocarbon-'dead' lignite (coal) present in Palaeogene mudstones within the catchment of Lago Fagnano contaminates the lacustrine dissolved inorganic carbon (DIC) pool, and therefore limits the reliable radiocarbon dating of the lake sediments (Moy *et al.*, 2011; and references therein). By comparing radiocarbon ages of bulk organic sediments, terrestrial macrofossils and pollen concentrates from the eastern-basin core LF06-PC18 (Fig. S1), Moy *et al.* (2011) identified a 5000 to 7000 cal yr offset of bulk organic ages to corresponding pollen dates. Similarly, terrestrial macrofossils produced apparently erroneous old ages, most likely due to remobilization from the basin slopes. Due to the isotopic equilibrium of trees and pollen with the atmospheric radiocarbon pool, therefore, dating of pollen concentrates produced the most accurate Holocene chronology for Lago Fagnano with a minimum error estimate of less than 300 cal yr (Moy *et al.*, 2011). However, despite applying a similar protocol for pollen extraction as in Moy *et al.* (2011), in the six samples from cores LF06-PC5 and LF06-PC17 analysed here, relative pollen amounts of only 10 to 60% could be obtained (Table 2). Significant proportions of non-pollen organic micro-remains, i.e. plant tissues, charred particles, algae and fungal residues (Table 2), likely contaminate these samples with old carbon. Thereby, the ^{14}C-depleted carbon is

incorporated in aquatic plants from the lake DIC pool that can have received old DIC from groundwater or bedrock meteorization (e.g. Abbott & Stafford, 1996; Albéric *et al.*, 2016). The high amount of charred particles (20 to 50%) in the samples suggests that erosion and influx of old particulate organic carbon from peat, soil and coal-bearing bedrock of the drainage basin to the lake is a further, probably even more important, source of contamination. Consequently, radiocarbon ages of all six samples turned out to be implausible, showing offsets of *ca* 2000 to 12 000 cal yr to the corresponding expected ages based on the H1 Hudson tephra (Stern *et al.*, 2016) for core LF06-PC5 and event-layer correlation for core LF06-PC17 (Waldmann *et al.*, 2011; Tables 1 and 2; Figs 2 and S1). Similar radiocarbon dating problems due to the presence of radiocarbon-dead lignite have been previously noted in other sites in Patagonia (Ariztegui *et al.*, 2007).

Therefore, linear age-depth models were established here for both investigated sediment cores assuming constant but different sedimentation rates for the two sub-basins, following the approach of Waldmann *et al.* (2010a, 2011). The H1 Hudson tephra age (calibrated to 8469 ± 39 cal yr BP) is well-constrained by ^{14}C dating in numerous outcrops, peat bogs and lakes in the region, where no freshwater reservoir effects were encountered (Stern, 2008; Stern *et al.*, 2016). This chronostratigraphic anchor provides the only available independent age control for Lago Fagnano sediments in the western sub-basin. It constrains the onset of sediment lamination in the western basin (LF06-PC5) at the early Holocene *ca* 10 900 cal yr BP, which corresponds well with glacial evolution in this region (Coronato *et al.*, 2009).

For the eastern sub-basin, the event stratigraphy correlated between cores LF06-PC17 (this study) and LF06-PC16 (Waldmann *et al.*, 2011) is reasonable (Fig. S1). Transferring the published pollen ages of core LF06-PC18 (Moy *et al.*, 2011; Fig. S1) to core LF06-PC17, however, is not straightforward and reveals an offset of the pollen dates of *ca* 400 to 700 cal yr to the event-derived estimations. This offset is close to the reported average *ca* 300 yr error of pollen ages (Moy *et al.*, 2011), but it may also indicate slight contamination of these samples.

Even though no significant long-term trends or changes in the XRF profiles of detrital elements (for example, K and Ti in Fig. 2) or in grain size are observed in the laminated sediments, the assumption of constant long-term sedimentation bears some uncertainty, preventing further interpretation. A thorough climate discussion for the region could only be done using varved lake sediments or tree ring records that are, however, so far not available in the area. Additional independent age control, for example from further tephra time markers, would be needed.

Lago Fagnano sediment record

X-ray fluorescence (XRF) element scanning of lacustrine sediment cores is a valuable and widely used tool to characterize lithological changes through time, and decipher underlying catchment-related and lake-internal processes (see, for example, contributions in Croudace & Rothwell, 2015). Supported by PCA, thin section microscopy, XRD and SEM analyses, as well as Fe and Mn speciation (the latter provided in Ordoñez *et al.*, 2020), the following inferences are drawn from the XRF dataset of the Lago Fagnano sediment cores under focus in this study.

The overall homogeneous grain size and clastic composition of the light grey clayey-silty mud, as reflected in XRF logs (Fig. 2), implies a relatively stable long-term supply of detrital sediments to Lago Fagnano during the Holocene. Clastic sediments are predominantly delivered by fluvial runoff, which in turn controls the sediment accumulation rates in the lake. In previous studies, the Fe content in Lago Fagnano sediments was interpreted as an indirect proxy for precipitation (Waldmann *et al.*, 2010a). However, the PCAs of XRF data from cores LF06-PC5 and LF06-PC17 (Fig. 4) demonstrate a diagenetic alteration of the Fe signal. Therefore, lithogenic elements that are inert to early diagenetic processes at neutral pH, i.e. Al, Si, K, Ti, Rb or Zr (Davies *et al.*, 2015), are more appropriate to use as indicators for precipitation changes at Lago Fagnano.

The constant slight decrease of Al, Si and K, which may indicate a decrease in clay minerals, along with declining density (Fig. 2A) may be related either to diminishing influx of suspended particles from glacial meltwater or to the development of vegetation and soils during the Holocene leading to reduced erosion from the catchment. The latter would be supported by palynology, reporting the progressive establishment of *Nothofagus* forest in the Fagnano watershed (Waldmann *et al.*, 2014). This is accompanied by the overall increasing trend of lake productivity and nutrient supply to Lago Fagnano during the Holocene, shown by bulk organic C and N curves (Waldmann

et al., 2010a; Moy *et al.*, 2011). The S and inc/coh logs of core LF06-PC5 (Fig. 2) follow this increasing trend during the studied time interval, which suggests a correlation with the organic carbon content of the sediments. Indeed, S is related to enriched organic matter (e.g. Passier *et al.*, 1999; Thomson *et al.*, 2006), and the XRF inc/coh scattering ratio has been shown to be a useful proxy for the organic content of sediments (Burnett *et al.*, 2011). It has to be stressed, though, that the lake maintained an ultra-oligotrophic to oligotrophic status throughout the Holocene (Waldmann *et al.*, 2014) and, in concert with a deep oxygenation of the lake, the preservation of any organic matter in the sediments is very poor leading to overall low total organic carbon (TOC) values (Fig. S1).

Formation and preservation of Fe/Mn-laminae

Waldmann *et al.* (2014) suggested that the cyclic alternation of light-grey clay and black/greenish laminae indicate sedimentation in a well-stratified lake, which might have induced anoxic or dysoxic conditions at the sediment–water interface. Fluctuations of redox-sensitive elements in the XRF data, where detrital elements and Mn/Fe are enriched in the light grey sediment, and Fe/K, S and As peaks depict black and greenish laminae (Figs 5 and 6), confirm that laminae formation in Lago Fagnano is related to redox processes, but not necessarily triggered by lake stratification. The following paragraphs will first discuss the processes ongoing at the sediment–water interface at water depths of 126 m (LF06-PC5). Then, this understanding will be used to depict potential preserved palaeo-redox fronts, followed by the discussion of the laminae formation and preservation in the Holocene Fagnano sediments.

The active redox front

The orange-brown Fe-oxide layers and brownish-black Mn-oxide patches, detected in the top *ca* 5 cm of the western-basin core LF06-PC5 (Fig. 5), are interpreted to have formed at the active redox front (Fig. 7A). Such a redox boundary develops, when dissolved Mn(II) and Fe(II) diffuse upward within reduced sediments, and oxidize to Mn(IV) and Fe(III) as soon as the O_2 concentration sufficiently increases (e.g. Davison, 1993; Torres *et al.*, 2014). Because the dark-brownish Mn-oxide accumulations are located in the topmost sediments, it can be assumed that O_2 penetration into the sediments is restricted, and that the oxic–anoxic interface is positioned at the sediment–water boundary in Lago Fagnano. Mn(II) is more soluble than Fe(II) and, hence, O_2 from the water column is consumed to build MnO_2, whereas Fe(II) is oxidized from Mn(IV) leading to Mn reduction and the accumulation of an Fe-oxide layer immediately below the Mn-enriched layer (e.g. Brown *et al.*, 2000; Och *et al.*, 2012). Indeed, Mn and Fe concentrations obtained by dissolution of metal-oxyhydroxides reach highest values within the Fagnano record, with 1.7 wt% (0 to 2 cm depth) and 3.1 wt% (2 to 6 cm depth), respectively (Ordoñez *et al.*, 2020). Arsenic, strongly enhanced within the Fe-oxide layer (Fig. 5), is affected by similar post-depositional diagenetic remobilization processes (Farmer & Lovell, 1986; Ordoñez *et al.*, 2020). Under oligotrophic

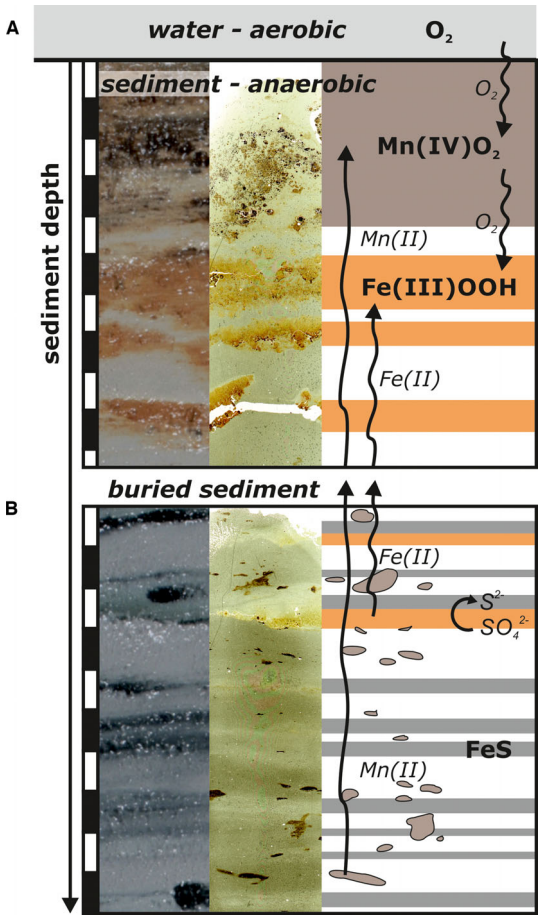

Fig. 7. (A) Mechanism of formation of an active, dynamically growing redox front, and (B) early diagenetic dissolution of palaeo-redox fronts (orange) and partial pyritization in black laminae (grey) in the sedimentary record of Lago Fagnano.

conditions, deep oxygenation of the hypolimnion, and constantly low sediment accumulation rates (*ca* 0.1 mm yr^{-1} in LF06-PC5), this Fe/Mn-oxide layer will dynamically grow and move upward with sedimentation, following the water–sediment redox interface. A change in these conditions can induce the preservation of the Fe/Mn-oxide front into deeper sediments and subsequently, the initiation of a new dynamic Fe/Mn-layer at the re-established O_2−Mn(II) front closer to the sediment–water interface (e.g. Granina *et al.*, 2004; Och *et al.*, 2012; Torres *et al.*, 2014).

Palaeo-redox front preservation and greenish laminae

A sudden increase in sedimentation rate would lead to a larger diffusive pathway and separate the O_2–Mn(II) interface. A similar process has been described in Lake Baikal and Lake Ohrid, where Fe/Mn-layers in the sedimentary record are suggested as markers of rapid changes of sedimentation regimes in periods of low sedimentation rates and well-oxygenated water column (Granina *et al.*, 2004; Vogel *et al.*, 2010). A rapid increase in sedimentation is a plausible mechanism to explain the particularly well-preserved greenish Fe/Mn-laminae underlying mass-wasting events in Lago Fagnano (Fig. 6B), leading to their interpretation as ancient redox fronts. This is supported by elevated levels of Fe^{3+} and Mn^{4+} from oxyhydroxides (0.86 wt% and 0.03 wt%, respectively) measured below a turbidite deposit (#5-1 in the western basin core LF06-PC5), even though these levels are significantly lower than in the active redox front (Ordoñez *et al.*, 2020). Such enrichments triggered by catastrophic sedimentation events have been described for example in the Saguenay Fjord, Canada (Mucci & Edenborn, 1992; Deflandre *et al.*, 2002). Many more greenish laminae showing distinct Fe-peaks occur independently of mass-transport deposits throughout both sediment profiles in cores LF06-PC5 and LF06-PC17 from both sub-basins (Figs 5 to 7). It appears most likely that these green layers represent palaeo-redox fronts that were buried when clastic sedimentation rates suddenly increase. The trigger for such abrupt increased sedimentation will be discussed further below.

Preservation of the active redox front at the sediment–water interface might also result from a steady-state process of increasingly slower, and at some point limited, reductive dissolution when the active Fe/Mn-layer grows. Och *et al.* (2012) suggested this mechanism as an alternative explanation for the cyclic pattern of Fe/Mn-layers in Lake Baikal. They proposed that a new active front evolves at the O_2–Mn(II) redox boundary along with the burial of the old Fe/Mn-layer, which then slowly dissolves and feeds the new redox boundary closer to the sediment–water interface. This process cannot be ruled out as explanation for the preservation of redox fronts in Lago Fagnano, and is not related to singular, potentially climate-driven events, in contrast to the mechanism illustrated above.

Potential mechanisms behind black laminae formation

The majority of laminae in both described cores of Lago Fagnano are black layers with only minor increases in redox-sensitive elements Fe, As and S. These layers do not represent palaeo-redox fronts, but their formation is potentially driven by small changes in bottom-water oxygenation due to reduced ventilation, and/or higher productivity. Changes in lake productivity would lead to enhanced organic matter production along with high oxygen consumption caused by its degradation in the water column and/or in the sediment. Major changes in lake productivity can be triggered by increased nutrient input through wind strength, changes in water supply or lake regime, or by increased temperatures; these processes may all lead to seasonal stratification in temperate lakes (Davison, 1993; Brown *et al.*, 2000; Katsev *et al.*, 2017). Seasonal mixing and stratification are the main drivers for the formation and preservation of annual laminations in many lakes, for example in oligotrophic Swedish lakes, where seasonal precipitation of Fe hydroxides and sulphides leads to characteristic colour-banding of the varved sediments (e.g. Renberg, 1986; Shchukarev *et al.*, 2008; Gälman *et al.*, 2009). In the case of Lago Fagnano, episodic stratification promoted by changing wind regime can possibly explain the formation of black laminae. The presence of broken littoral diatom frustules throughout the light and dark sediment layers in the deep basins (Waldmann, 2008; Waldmann *et al.*, 2014) indicates recycling of sediments from shallow areas of the lake due to persisting wind-driven wave activity and mixing. However, longer-term monitoring data that could rule out an episodic stratification do not exist from Lago Fagnano.

Enhanced mass accumulation rate of settling organic matter, due to higher biological productivity and/or increased influx, would also lead to stronger oxygen consumption in the

sediment. Floods carrying high amounts of organic matter were suggested to trigger this mechanism in Lake Storsjön (Sweden), where black organic-rich layers were preserved in the sediments that are enriched in Fe sulphides (Labuhn *et al.*, 2018). In Lago Fagnano, peaks in the inc/coh ratio from XRF data (Figs 5 and 6) indeed suggest a slightly higher organic carbon content in some of the black laminae observed (Fig. 5A). The common association of arsenic with organic matter supports this direction. However, because the overall TOC content of <1.2% (Waldmann *et al.*, 2010a) is very low and as organic enrichment is not observed in thin sections, it can only be suggested that this mechanism may explain the formation of black laminae.

Partial dissolution and pyritization

Early diagenetic processes, in particular reductive dissolution, lead to an obscured preservation of ancient Fe/Mn-layers in the form of greenish laminae in Lago Fagnano sediments. The disappearance of black laminae when oxidation occurs, along with their patchy occurrence down-core also suggests specific microbial processes that can enlighten laminae formation and preservation.

Although clear Mn-layers can be distinguished at the top of the core (Figs 5B and 7A), they are rarely identified as proper laminae down-core, and rather appear as patchy enrichments after the cores were oxidized (Figs 5C and 7B). A similar pattern is observed for Fe-layers in the deeper parts of the core, where Fe-oxide layers are only preserved as thin greenish laminae. Both greenish and black Fe-rich laminae are often enriched in S and As, which is uniquely observed under XRF and μXRF scans. Arsenic can be incorporated into FeS_2 (Peterson & Carpenter, 1986; Huerta-Diaz & Morse, 1992) and Fe-oxyhydroxides, as empirically demonstrated for Lago Fagnano sediments by Ordoñez *et al.* (2020). Trace elements such as Ni and Co show diagenetic enrichment along with the reduced Fe fraction only, suggesting the presence of mineralized sulphide phases even though XRD or SEM data did not confirm the presence of pyrite. Instead, quick disappearance of black laminae after opening the cores (Figs 5C and 6C) suggests that there was rapid oxidation of unstable Fe-sulphide phases like amorphous Fe-(mono)sulphide, mackinawite or greigite, which are precursors of pyrite.

Bacterial sulphate reduction might be responsible for the production of sulphides that subsequently reduces Fe-phases and leads to the partial dissolution of Fe-oxide laminae and the formation of Fe-sulphide minerals through the reaction of Fe^{2+} and sulphides (e.g. Berner, 1970, 1984, 1985; Burdige, 1993; Fig. 7B). The absence of pyrite however indicates that the sulphidization of the sediments is limited, and rather results in the partial pyritization and preservation of intermediate phases (Richter *et al.*, 2006). In oligotrophic lacustrine environments, and particularly in Lago Fagnano, where sulphate is depleted in the water body, the relatively limited amount of primary production associated with low sulphate levels may be the limiting factor for sulphate reduction activity (Berner, 1984; Holmer & Storkholm, 2001). Therefore, although Fe^{2+} may be available, the relative lack of sulphide or sulphate in general prevents complete pyritization of the sediment, even in black laminae that may potentially be enriched in organic matter. Excess ferrous Fe that cannot react with sulphide may diffuse away and reduce manganese oxides as suggested by Och *et al.* (2012) in Lake Baikal, resulting in the associated loss of Mn downward through the sedimentary profile. In Lago Fagnano, a thorough follow-up study of active microbial communities and biogeochemical cycles will be needed to validate controlling factors over Fe/Mn-lamina dissolution and preservation.

Potential forcing of the lamination pattern

The ultimate trigger for the preservation of Fe/Mn-redox fronts as thin greenish laminae in the sediments of Lago Fagnano cannot be unequivocally determined by the approach applied here. However, based on the identification of similar behaviours in palaeo-redox fronts underlying (earthquake-related) event beds, the rapid and recurrent increase in sedimentation rates also due to other triggers than such events is suggested here as the most likely mechanism behind the preservation of Fe/Mn-redox fronts in Lago Fagnano. Enhanced sediment influx may also be forced by higher runoff related to increased precipitation in the lake's watershed (Waldmann *et al.*, 2010a). This would support the observation at Lago Fagnano from the early summer in 2006, when an unusually high lake level causing flooding and erosion of coastal areas may have led to a sudden increase of detrital material in the water column and mixing of the lake (Waldmann *et al.*, 2014). Because wind strength and rainfall amount in Tierra del Fuego are mostly controlled by the Southern Hemisphere Westerlies (SHW; e.g. Moreno *et al.*, 2018), the strength and latitudinal position of this wind belt may predominantly govern

the decadal–centennial scale recurrence of greenish Fe-oxide layers in the sediment records of the two sub-basins of Lago Fagnano, with stronger winds and rainfall favouring higher sedimentation and preservation of these redox fronts. In contrast, black laminae, which likely result from a temporarily reduced bottom water oxygenation due to shallower ventilation of the water body, may be rather related to weaker winds and less precipitation. However, answering the question of whether the Lago Fagnano lamination is triggered by SHW oscillations, any other climate oscillations, solar forcing or partially by a process that is not climatically driven (Och *et al.*, 2012), cannot ultimately be answered here due to the lack of a solid chronology.

CONCLUSIONS

The Holocene sedimentary record of Lago Fagnano in Tierra del Fuego preserves a succession of continuous lamination despite deep mixing of the water column, which today is forced by year-round prevailing strong Southern Hemisphere Westerly winds. Applying high-resolution sediment–geochemical analyses allowed deciphering the mechanisms of laminae formation and preservation in Lago Fagnano. Very thin black and greenish laminae within predominantly clastic sediments show distinct but different fluctuations in redox-sensitive elements, such as Fe, Mn, S and As, which led to the assumption that these two laminae-types are related to different redox processes. Greenish Fe-oxide laminae are proposed to be remnants of palaeo-redox fronts. Such Fe/Mn-redox fronts at the sediment–water interface were most likely buried through rapid increases of sedimentation rates related to higher runoff to the lake when the Southern Hemisphere Westerlies are stronger. Black Fe-sulphide laminae occur most likely due to changing bottom water oxygen levels through slight fluctuations of biological productivity and/or ventilation depth, impacting lamination at the millimetre-scale. A significant challenge of this study was the poor preservation of green and black laminae after their burial, due to early diagenetic processes like reductive dissolution and partial pyritization, involving complex biogeochemical element cycling. Processes related to changing redox conditions and the preservation/diagenesis of sedimentary Fe/Mn-layers in Lago Fagnano might well serve as an analogue for palaeo-redox fronts in similar oligotrophic, deep-water and deeply oxygenated lacustrine settings. This study demonstrates the great value of high-resolution elemental analysis on continuously laminated sediments from climatically-susceptible lacustrine systems for better understanding the controlling source-to-sink mechanisms in lakes.

ACKNOWLEDGEMENTS

We express our gratitude to the editor and reviewers, who greatly improved the quality of this manuscript through helpful discussions. This project has received funding from the European Union's Horizon 2020 research and innovation programme under the Marie Skłodowska-Curie grant agreement No. 706244, and from the Swiss National Science Foundation SNSF (grant No. 200021_166308/1). We thank Hendrik Vogel and Flavio Anselmetti (University of Bern) for hospitality and assistance during ITRAX-XRF measurements, Agathe Martignier (University of Geneva) for assisting the SEM, Michael Köhler (MKfactory, Stahnsdorf) for thin section preparation, Michèle Dinies (Freie Universität Berlin) for pollen extraction, and Rik Tjallingii (GFZ Potsdam) for advice in XRF data processing. We declare that there is no conflict of interest concerning this research.

DATA AVAILABILITY STATEMENT

Data of this article will be publicly available on the GFZ Data Services Portal (https://dataservices.gfz-potsdam.de/portal/).

REFERENCES

Abbott, M.B. and **Stafford, T.W.** (1996) Radiocarbon geochemistry of modern and ancient Arctic lake systems, Baffin Island, Canada. *Quat. Res.*, **45**, 300–311.

Albéric, P., **Jézéquel, D.**, **Bergonzini, L.**, **Chapron, E.**, **Viollier, E.**, **Massault, M.** and **Michard, G.** (2016) Carbon cycling and organic radiocarbon reservoir effect in a meromictic crater lake (Lac Pavin, Puy-de-Dôme, France). *Radiocarbon*, **55**, 1029–1042.

Ariztegui, D., **Bösch, P.** and **Davaud, E.** (2007) Dominant ENSO frequencies during the Little Ice Age in Northern Patagonia: the varved record of proglacial Lago Frías, Argentina. *Quat. Int.*, **161**, 46–55.

Berner, R.A. (1970) Sedimentary pyrite formation. *Am. J. Sci.*, **268**, 1–23.

Berner, R.A. (1984) Sedimentary pyrite formation: an update. *Geochim. Cosmochim. Acta*, **48**, 605–615.

Berner, R.A. (1985) Sulphate reduction, organic matter decomposition and pyrite formation. *Philos. Trans. R. Soc. Lond. Ser. A Math. Phys. Sci.*, **315**, 25–38.

Boyle, J.F. (2001) Inorganic geochemical methods in palaeolimnology. In: *Tracking Environmental Change*

Using Lake Sediments (Eds Last, W. and Smol, J.), Developments in Paleoenvironmental Research, **2**, pp. 83–141. Springer, Dordrecht Netherlands.

Bradley, R.S. (1999) *Paleclimatology - Climates of the Quaternary*, 2nd edn. Elsevier Academic Press, San Diego, US.

Brauer, A., **Endres, C.** and **Negendank, J.F.W.** (1999) Lateglacial calendar year chronology based on annually laminated sediments from Lake Meerfelder Maar, Germany. *Quat. Int.*, **61**, 17–25.

Brown, E.T., **Le Callonnec, L.** and **German, C.R.** (2000) Geochemical cycling of redox-sensitive metals in sediments from Lake Malawi: a diagnostic paleotracer for episodic changes in mixing depth. *Geochim. Cosmochim. Acta*, **64**, 3515–3523.

Brown, T.A., **Nelson, D.E.**, **Mathewes, R.W.**, **Vogel, J.S.** and **Southon, J.R.** (1989) Radiocarbon dating of pollen by accelerator mass spectrometry. *Quat. Res.*, **32**, 205–212.

Bryant, C.L., **Farmer, J.G.**, **MacKenzie, A.B.**, **Bailey-Watts, A.E.** and **Kirika, A.** (1997) Manganese behavior in the sediments of diverse Scottish freshwater lochs. *Limnol. Oceanogr.*, **42**, 918–929.

Burdige, D.J. (1993) The biogeochemistry of manganese and iron reduction in marine sediments. *Earth-Sci. Rev.*, **35**, 249–284.

Burnett, A.P., **Soreghan, M.J.**, **Scholz, C.A.** and **Brown, E.T.** (2011) Tropical East African climate change and its relation to global climate: a record from Lake Tanganyika, Tropical East Africa, over the past 90+kyr. *Palaeogeog. Palaeoclimatol. Palaeoecol.*, **303**, 155–167.

Corella, J.P., **Brauer, A.**, **Mangili, C.**, **Rull, V.**, **Vegas-Vilarrúbia, T.**, **Morellón, M.** and **Valero-Garcés, B.L.** (2012) The 1.5-ka varved record of Lake Montcortès (southern Pyrenees, NE Spain). *Quat. Res.*, **78**, 323–332.

Coronato, A., **Seppälä, M.**, **Ponce, J.F.** and **Rabassa, J.** (2009) Glacial geomorphology of the Pleistocene Lake Fagnano ice lobe, Tierra del Fuego, southern South America. *Geomorphology*, **112**, 67–81.

Croudace, I.W., **Rindby, A.** and **Rothwell, R.G.** (2006) ITRAX: description and evaluation of a new multi-function X-ray core scanner. *Geol. Soc. Lond. Spec. Publ.*, **267**, 51–63.

Croudace, I.W. and **Rothwell, R.G.** (2015) *Micro-XRF Studies of Sediment Cores: Applications of a Non-destructive Tool for the Environmental Sciences*. Springer Science, Dordrecht, 688 pp.

Davies, S.J., **Lamb, H.F.** and **Roberts, S.J.** (2015) Micro-XRF core scanning in palaeolimnology: recent developments. In: *Micro-XRF Studies of Sediment Cores* (Eds Croudace, I.W. and Rothwell, R.G.), Developments in Paleoenvironmental Research, **17**, pp. 189–226. Springer, Dordrecht Netherlands.

Davison, W. (1993) Iron and manganese in lakes. *Earth-Sci. Rev.*, **34**, 119–163.

Deflandre, B., **Mucci, A.**, **Gagné, J.-P.**, **Guignard, C.** and **Sundby, B.** (2002) Early diagenetic processes in coastal marine sediments disturbed by a catastrophic sedimentation event. *Geochim. Cosmochim. Acta*, **66**, 2547–2558.

Deike, R.G., **Granina, L.**, **Callender, E.** and **McGee, J.J.** (1997) Formation of ferric iron crusts in quaternary sediments of Lake Baikal, Russia, and implications for paleoclimate. *Mar. Geol.*, **139**, 21–46.

Farmer, J.G. (1994) Environmental change and the chemical record in Loch Lomond sediments. *Hydrobiologia*, **290**, 39–49.

Farmer, J.G. and **Lovell, M.A.** (1986) Natural enrichment of arsenic in Loch Lomond sediments. *Geochim. Cosmochim. Acta*, **50**, 2059–2067.

Francus, P., **von Suchodoletz, H.**, **Dietze, M.**, **Donner, R.V.**, **Bouchard, F.**, **Roy, A.-J.**, **Fagot, M.**, **Verschuren, D.** and **Kröpelin, S.** (2013) Varved sediments of Lake Yoa (Ounianga Kebir, Chad) reveal progressive drying of the Sahara during the last 6100 years. *Sedimentology*, **60**, 911–934.

Gaiero, D.M., **Probst, J.L.**, **Depetris, P.J.**, **Bidart, S.M.** and **Leleyter, L.** (2003) Iron and other transition metals in Patagonian riverborne and windborne materials: geochemical control and transport to the southern South Atlantic Ocean. *Geochim. Cosmochim. Acta*, **67**, 3603–3623.

Gälman, V., **Rydberg, J.**, **Shchukarev, A.**, **Sjöberg, S.**, **Martínez-Cortizas, A.**, **Bindler, R.** and **Renberg, I.** (2009) The role of iron and sulfur in the visual appearance of lake sediment varves. *J. Paleolimnol.*, **42**, 141–153.

Garreaud, R., **Lopez, P.**, **Minvielle, M.** and **Rojas, M.** (2013) Large-scale control on the patagonian climate. *J. Clim.*, **26**, 215–230.

Gong, D. and **Wang, S.** (1999) Definition of antarctic oscillation index. *Geophys. Res. Lett.*, **26**, 459–462.

Granina, L., **Karabanov, E.** and **Callender, E.** (1993) Relics of oxidized ferromanganese formations in the bottom sediments of Lake Baikal. *IPPCCE Newsl.*, **7**, 32–39.

Granina, L.Z., **Mats, V.D.** and **Phedorin, M.A.** (2010) Iron-manganese formations in the Baikal region. *Russ. Geol. Geophys.*, **51**, 650–660.

Granina, L., **Müller, B.** and **Wehrli, B.** (2004) Origin and dynamics of Fe and Mn sedimentary layers in Lake Baikal. *Chem. Geol.*, **205**, 55–72.

Granina, L.Z., **Zakharova, Y.P.** and **Parfenova, V.V.** (2011) Biogenic Fe and Mn accumulation in the bottom sediments of Lake Baikal. *Geochem. Int.*, **49**, 1154.

Haberzettl, T., **Corbella, H.**, **Fey, M.**, **Janssen, S.**, **Lücke, A.**, **Mayr, C.**, **Ohlendorf, C.**, **Schäbitz, F.**, **Schleser, G.H.**, **Wille, M.**, **Wulf, S.** and **Zolitschka, B.** (2007) Lateglacial and Holocene wet—dry cycles in southern Patagonia: chronology, sedimentology and geochemistry of a lacustrine record from Laguna Potrok Aike, Argentina. *Holocene*, **17**, 297–310.

Holmer, M. and **Storkholm, P.** (2001) Sulphate reduction and sulphur cycling in lake sediments: a review. *Freshw. Biol.*, **46**, 431–451.

Huerta-Diaz, M.A. and **Morse, J.W.** (1992) Pyritization of trace metals in anoxic marine sediments. *Geochim. Cosmochim. Acta*, **56**, 2681–2702.

Katsev, S., **Verburg, P.**, **Llirós, M.**, **Minor, E.C.**, **Kruger, B.R.** and **Li, J.** (2017) Tropical meromictic lakes: specifics of meromixis and case studies of Lakes Tanganyika, Malawi, and Matano. In: *Ecology of Meromictic Lakes* (Eds Gulati, R.D., Zadereev, E.S. and Degermendzhi, A.G.), pp. 277–323. Springer International Publishing, Cham.

Labuhn, I., **Hammarlund, D.**, **Chapron, E.**, **Czymzik, M.**, **Dumoulin, J.-P.**, **Nilsson, A.**, **Régnier, E.**, **Robygd, J.** and **von Grafenstein, U.** (2018) Holocene hydroclimate variability in central Scandinavia inferred from flood layers in Contourite Drift Deposits in Lake Storsjön. *Quaternary*, **1**, 1–24.

Lamy, F., **Hebbeln, D.**, **Röhl, U.** and **Wefer, G.** (2001) Holocene rainfall variability in southern Chile: a marine record of latitudinal shifts of the Southern Westerlies. *Earth Planet. Sci. Lett.*, **185**, 369–382.

Lau, M.P., **Niederdorfer, R.**, **Sepulveda-Jauregui, A.** and **Hupfer, M.** (2018) Synthesizing redox biogeochemistry at aquatic interfaces. *Limnologica*, **68**, 59–70.

Löwemark L., **Bloemsma M.**, **Croudace I.**, **Daly J.S.**, **Edwards R.J.**, **Francus P.**, **Galloway J.M.**, **Gregory B.R.B.**, **Steven Huang J.-J.**, **Jones A.F.**, **Kylander M.**, **Luo Y.**, **Maclachlan S.**, **Ohlendorf C.**, **Patterson R.T.**, **Pearce C.**, **Profe J.**, **Reinhardt E.G.**, **Stranne C.**, **Tjallingii R.**, **Turner J.N.** (2019) Practical guidelines and recent advances in the Itrax XRF core-scanning procedure. *Quat Int*, **514**, 16–29.

Moreno, P.I., **Vilanova, I.**, **Villa-Martínez, R.**, **Dunbar, R.B.**, **Mucciarone, D.A.**, **Kaplan, M.R.**, **Garreaud, R.D.**, **Rojas, M.**, **Moy, C.M.**, **De Pol-Holz, R.** and **Lambert, F.** (2018) Onset and evolution of southern annular mode-like changes at centennial timescale. *Sci. Rep.*, **8**, 3458.

Moy, C.M., **Dunbar, R.B.**, **Guilderson, T.P.**, **Waldmann, N.**, **Mucciarone, D.A.**, **Recasens, C.**, **Ariztegui, D.**, **Austin Jr, J.A.** and **Anselmetti, F.S.** (2011) A geochemical and sedimentary record of high southern latitude Holocene climate evolution from Lago Fagnano, Tierra del Fuego. *Earth Planet. Sci. Lett.*, **302**, 1–13.

Mucci, A. and **Edenborn, H.M.** (1992) Influence of an organic-poor landslide deposit on the early diagenesis of iron and manganese in a coastal marine sediment. *Geochim. Cosmochim. Acta*, **56**, 3909–3921.

Müller, B., **Granina, L.**, **Schaller, T.**, **Ulrich, A.** and **Wehrli, B.** (2002) P, As, Sb, Mo, and other elements in sedimentary Fe/Mn layers of lake Baikal. *Environ. Sci. Technol.*, **36**, 411–420.

Naeher, S., **Gilli, A.**, **North, R.P.**, **Hamann, Y.** and **Schubert, C.J.** (2013) Tracing bottom water oxygenation with sedimentary Mn/Fe ratios in Lake Zurich, Switzerland. *Chem. Geol.*, **352**, 125–133.

Nakagawa, T., **Brugiapaglia, E.**, **Digerfeldt, G.**, **Reille, M.**, **Beaulieu, J.-L.-D.** and **Yasuda, Y.** (1998) Dense-media separation as a more efficient pollen extraction method for use with organic sediment/deposit samples: comparison with the conventional method. *Boreas*, **27**, 15–24.

Och, L.M., **Müller, B.**, **Voegelin, A.**, **Ulrich, A.**, **Göttlicher, J.**, **Steiniger, R.**, **Mangold, S.**, **Vologina, E.G.** and **Sturm, M.** (2012) New insights into the formation and burial of Fe/Mn accumulations in Lake Baikal sediments. *Chem. Geol.*, **330**, 244–259.

Olivero, E.B. and **Martinioni, D.R.** (2001) A review of the geology of the Argentinian Fuegian Andes. *J. S. Am. Earth. Sci.*, **14**, 175–188.

Ordoñez, L.G., **Neugebauer, I.**, **Thomas, C.**, **Chiaradia, M.**, **Waldmann, N.** and **Ariztegui, D.** (2020) Sediment redox dynamics in an oligotrophic deep-water lake in Tierra del Fuego: insights from Fe isotopes. *EarthArXiv*-Preprint. https://doi.org/10.31223/osf.io/j5md2

Passier, H.F., **Middelburg, J.J.**, **de Lange, G.J.** and **Böttcher, M.E.** (1999) Modes of sapropel formation in the eastern Mediterranean: some constraints based on pyrite properties. *Mar. Geol.*, **153**, 199–219.

Peterson, M.L. and **Carpenter, R.** (1986) Arsenic distributions in porewaters and sediments of Puget Sound, Lake Washington, the Washington coast and Saanich Inlet, B.C. *Geochim. Cosmochim. Acta*, **50**, 353–369.

Quirós, R. and **Drago, E.** (1999) The environmental state of Argentinean lakes: an overview. *Lakes Reserv. Sci. Policy Manag. Sustain. Use*, **4**, 55–64.

Regnéll, J. and **Everitt, E.** (1996) Preparative centrifugation—a new method for preparing pollen concentrates suitable for radiocarbon dating by AMS. *Veg. Hist. Archaeobot.*, **5**, 201–205.

Renberg, I. (1986) Photographic demonstration of the annual nature of a varve type common in N. Swedish lake sediments. *Hydrobiologia*, **140**, 93–95.

Richter, T.O., **van der Gaast, S.**, **Koster, B.**, **Vaars, A.**, **Gieles, R.**, **de Stigter, H.C.**, **De Haas, H.** and **van Weering, T.C.E.** (2006) The Avaatech XRF Core Scanner: technical description and applications to NE Atlantic sediments. In: *New techniques in sediment core analysis* (Ed. Rothwell, R.G.), **267**, pp. 39–50. Geological Society Special Publications, London.

Rogers, J.C. and **Loon, H.V.** (1982) Spatial variability of sea level pressure and 500 mb height anomalies over the Southern Hemisphere. *Mon. WeatherRev.*, **110**, 1375–1392.

Shchukarev, A., **Gälman, V.**, **Rydberg, J.**, **Sjöberg, S.** and **Renberg, I.** (2008) Speciation of iron and sulphur in seasonal layers of varved lake sediment: an XPS study. *Surf. Interface Anal.*, **40**, 354–357.

Sobek, S., **Durisch-Kaiser, E.**, **Zurbrügg, R.**, **Wongfun, N.**, **Wessels, M.**, **Pasche, N.** and **Wehrli, B.** (2009) Organic carbon burial efficiency in lake sediments controlled by oxygen exposure time and sediment source. *Limnol. Oceanogr.*, **54**, 2243–2254.

Stern, C. (2008) Holocene tephrochronology record of large explosive eruptions in the southernmost Patagonian Andes. *Bull. Volcanol.*, **70**, 435–454.

Stern, C.R., **Moreno, P.I.**, **Henríquez, W.I.**, **Villa-Martínez, R.**, **Sagredo, E.**, **Aravena, J.C.** and **de Pol-Holz, R.** (2016) Holocene tephrochronology around Cochrane (~47°S), southern Chile. *Andean Geol.*, **43**, 1–19.

Tassone, A., **Lippai, H.**, **Lodolo, E.**, **Menichetti, M.**, **Comba, A.**, **Hormaechea, J.L.** and **Vilas, J.F.** (2005) A geological and geophysical crustal section across the Magallanes-Fagnano fault in Tierra del Fuego. *J. S. Am. Earth. Sci.*, **19**, 99–109.

Thomson, J., **Croudace, I.W.** and **Rothwell, R.G.** (2006) A geochemical application of the ITRAX scanner to a sediment core containing eastern Mediterranean sapropel units. In: *New Techniques in Sediment Core Analysis* (Ed. Rothwell, R.G.), **267**, pp. 65–77. Geological Society Special Publications, London.

Tjallingii, R., **Röhl, U.**, **Kölling, M.** and **Bickert, T.** (2007) Influence of the water content on X-ray fluorescence core-scanning measurements in soft marine sediments. *Geochem. Geophys. Geosyst.*, **8**(Q02004), 1–12.

Torres, N.T., **Och, L.M.**, **Hauser, P.C.**, **Furrer, G.**, **Brandl, H.**, **Vologina, E.**, **Sturm, M.**, **Burgmann, H.** and **Muller, B.** (2014) Early diagenetic processes generate iron and manganese oxide layers in the sediments of Lake Baikal, Siberia. *Environ. Sci. Process Impacts*, **16**, 879–889.

Vogel, H., **Wagner, B.**, **Zanchetta, G.**, **Sulpizio, R.** and **Rosén, P.** (2010) A paleoclimate record with tephrochronological age control for the last glacial-interglacial cycle from Lake Ohrid, Albania and Macedonia. *J. Paleolimnol.*, **44**, 295–310.

Waldmann, N. (2008) *Late Quaternary environmental changes in Lago Fagnano, Tierra del Fuego (54°S): reconstructing sedimentary processes, natural hazards and paleoclimate*. University of Geneva, Geneva, Switzerland, 188 pp.

Waldmann, N., **Anselmetti, F.S.**, **Ariztegui, D.**, **Austin, J.J.A.**, **Pirouz, M.**, **Moy, C.M.** and **Dunbar, R.** (2011) Holocene mass-wasting events in Lago Fagnano, Tierra del Fuego (54°S): implications for paleoseismicity of the Magallanes-Fagnano transform fault. *Basin Res.*, **23**, 171–190.

Waldmann, N., **Ariztegui, D.**, **Anselmetti, F.S.**, **Austin Jr, J.A.**, **Dunbar, R.**, **Moy, C.M.** and **Recasens, C.** (2008) Seismic stratigraphy of Lago Fagnano sediments (Tierra del Fuego, Argentina) - a potential archive of paleoclimatic change and tectonic activity since the Late Glacial. *Geol. Acta*, **6**, 101–110.

Waldmann, N., **Ariztegui, D.**, **Anselmetti, F.S.**, **Austin, J.A.**, **Moy, C.M.**, **Stern, C.**, **Recasens, C.** and **Dunbar, R.B.** (2010a) Holocene climatic fluctuations and positioning of the Southern Hemisphere westerlies in Tierra del Fuego (54°S), Patagonia. *J. Quat. Sci.*, **25**, 1063–1075.

Waldmann, N., **Ariztegui, D.**, **Anselmetti, F.S.**, **Coronato, A.** and **Austin Jr., J.A.** (2010b) Geophysical evidence of multiple glacier advances in Lago Fagnano (54°S), southernmost Patagonia. *Quat. Sci. Rev.*, **29**, 1188–1200.

Waldmann, N., **Borromei, A.M.**, **Recasens, C.**, **Olivera, D.**, **Martínez, M.A.**, **Maidana, N.I.**, **Ariztegui, D.**, **Austin, J.A.**, **Anselmetti, F.S.** and **Moy, C.M.** (2014) Integrated reconstruction of Holocene millennial-scale environmental changes in Tierra del Fuego, southernmost South America. *Palaeogeog. Palaeoclimatol. Palaeoecol.*, **399**, 294–309.

Weltje, G.J. and **Tjallingii, R.** (2008) Calibration of XRF core scanners for quantitative geochemical logging of sediment cores: theory and application. *Earth Planet. Sci. Lett.*, **274**, 423–438.

Manuscript received 6 December 2020; revision accepted 17 January 2022

Supporting Information

Additional information may be found in the online version of this article:

Figure S1. Event layer correlation between cores LF06-PC17 (this study), LF06-PC14 and LF06-PC16 (Waldmann *et al.*, 2011) and LF06-PC18 (Moy *et al.*, 2011).

Table S1. Correlation coefficients (R) of XRF element scanner data for laminated sections of cores LF06-PC5 (lower-left triangle) and LF06-PC17 (upper-right triangle).